Shallow geological structures triggered during the Mw 6.4 Meinong earthquake, southwestern Taiwan

M. Le Béon, M.-H. Huang, J. Suppe, S.-T. Huang, E. Pathier, W.-J. Huang, C.-L. Chen, B. Fruneau, S. Baize, K.-E. Ching, et al.

Terr. Atmos. Ocean. Sci., Vol. 28, No. 5, 663-681, October 2017 doi: 10.3319/TAO.2017.03.20.02

Shallow geological structures triggered during the M_w 6.4 Meinong earthquake, southwestern Taiwan

Maryline Le Béon[1, *], Mong-Han Huang[2, 3], John Suppe[4, 5], Shiuh-Tsann Huang[6], Erwan Pathier[7], Wen-Jeng Huang[8], Chien-Liang Chen[9], Bénédicte Fruneau[10], Stéphane Baize[11], Kuo-En Ching[12], and Jyr-Ching Hu[5]

[1] *Department of Earth Sciences, National Central University, Taoyuan City, Taiwan*
[2] *Department of Geology, University of Maryland, College Park, Maryland, U.S.A.*
[3] *NASA Jet Propulsion Laboratory, California Institute of Technology, Pasadena, California, USA*
[4] *Department of Earth and Atmospheric Sciences, University of Houston, Houston, Texas, USA*
[5] *Department of Geosciences, National Taiwan University, Taipei City, Taiwan*
[6] *Exploration and Development Research Institute, Chinese Petroleum Corporation, Miaoli, Taiwan*
[7] *Université Grenoble Alpes, Université Savoie Mont Blanc, CNRS, IRD, IFSTTAR, ISTerre, Grenoble, France*
[8] *Active Tectonics Division, Central Geological Survey, MOEA, New Taipei City, Taiwan*
[9] *Institute of Applied Geology, National Central University, Taoyuan City, Taiwan*
[10] *Université Paris-Est, LASTIG, IGN, UPEM, Marne-la-Vallée, France*
[11] *Institut de Radioprotection et de Sureté Nucléaire, Fontenay-aux-Roses, France*
[12] *Department of Geomatics, National Cheng-Kung University, Tainan City, Taiwan*

Article history:

Received 2 November 2016
Revised 13 March 2017
Accepted 20 March 2017

Keywords:

Active fault, Surface rupture, Coseismic deformation, Backthrust, Fault-related folding, Balanced cross-sections, InSAR, aseismic slip, Triggered slip, Gutingkeng mudstone

Citation:

Le Béon, M., M.-H. Huang, J. Suppe, S.-T. Huang, E. Pathier, W.-J. Huang, C.-L. Chen, B. Fruneau, S. Baize, K.-E. Ching, and J.-C. Hu, 2017: Shallow geological structures triggered during the M_w 6.4 Meinong earthquake, southwestern Taiwan. Terr. Atmos. Ocean. Sci., 28, 663-681, doi: 10.3319/TAO.2017.03.20.02

ABSTRACT

The Meinong earthquake generated up to ~10 cm surface displacement located 10 - 35 km west of the epicenter and monitored by InSAR and GPS. In addition to coseismic deformation related to the deep earthquake source, InSAR revealed three sharp surface displacement gradients. One of them is extensional and is inconsistent with the westward interseismic shortening of ~45 mm yr^{-1} in this region. The gradient sharpness suggests slip triggering on shallow structures, some of which were not well documented before. To characterize these shallow structures, we investigated potential surface ruptures in the field. Sets of ~NS tension cracks distributed over 25 - 300 m width, with cumulative extension in the same order as InSAR observations, were found along 5.5 km distance along the extensional gradient and are interpreted as surface rupture. We build two E-W regional balanced cross-sections, based on surface geology, subsurface data, and coseismic and interseismic geodetic data. From the Coastal Plain to the east edge of the coseismic deformation area, we propose a series of three active west-dipping backthrusts: the Houchiali fault, the Napalin-Pitou backthrust, and the Lungchuan backthrust. They all root on the 3.5 - 4.0 km deep Tainan detachment located near the base of the 3-km-thick Gutingkeng mudstone. Further east, the detachment would ramp down to ~7 km depth. Coseismic surface deformation measurements suggest that, in addition to the deeper (15 - 20 km) main rupture plane, mostly the ramp, the Lungchuan backthrust, and the Tainan detachment were activated during or right after the earthquake. Local extension is considered as transient deformation at the west edge of the shallow main slip zone.

1. INTRODUCTION

Ground surface ruptures with minor deformation (~0.1 - 10 cm) are sometimes reported on faults off moderate to large (M ~6 to 7) earthquake sources. This phenomenon has been referred to as triggered slip or coactive faulting. It was observed mostly in California [1968 Borrego Mountain: Allen et al. (1972); 1992 Landers earthquake sequence: Bodin et al. (1994) and Price and Sandwell (1998); 1994 Northridge: Cruikshank et al. (1996) and Johnson et al. (1996); 2010 El Mayor-Cucapah: Rymer et al. (2010) and Wei et al. (2011)],

* *Corresponding author*
E-mail: mlebeon@gmail.com

but also elsewhere in the world [1998 Fandoqa, Iran: Berberian et al. (2001); 1999 Izmit, Turkey: Wright et al. (2001); 1999 Chi-Chi, Taiwan: Pathier et al. (2003); 2016 Kumamoto, Japan: Goto et al. (2017)]. These faint features are not straightforward to observe in the field because they require detailed fieldwork away from the main rupture zone to discover very small ground deformation. Therefore, triggered slip likely occurs more often than effectively observed and in a greater variety of tectonic settings.

This study investigates the case of a moderate earthquake, the M_w 6.4 Meinong earthquake that struck southwestern Taiwan on 5 February 2016 (Fig. 1). The hypocenter was located at 15 - 23 km depth. Focal mechanisms from various institutions, aftershock distribution, and quick-response source modeling [Huang et al. 2016a; Lee et al. 2016; National Earthquake Information Center (NEIC) 2016; Wen et al. 2017; Central Weather Bureau (http://www.cwb.gov.tw)] pointed to a NW-SE fault plane dipping 25 - 30° to the northeast for the source of this event. In spite of moderate magnitude and significant depth, this earthquake generated surface deformation of > 10 cm monitored by GPS and Interferometric Synthetic Aperture Radar (InSAR) (Huang et al. 2016a), with the largest deformation area unexpectedly located 10 - 35 km west of the epicenter (Fig. 2). InSAR results also revealed three relatively sharp displacement gradients, oriented N5°E to N20°E, roughly parallel to surficial geological structures (Chinese Petroleum Corporation 1989). Joint inversion of seismic waveforms and geodetic data suggests the activation of an additional east-dipping thrust fault west of the epicenter, at

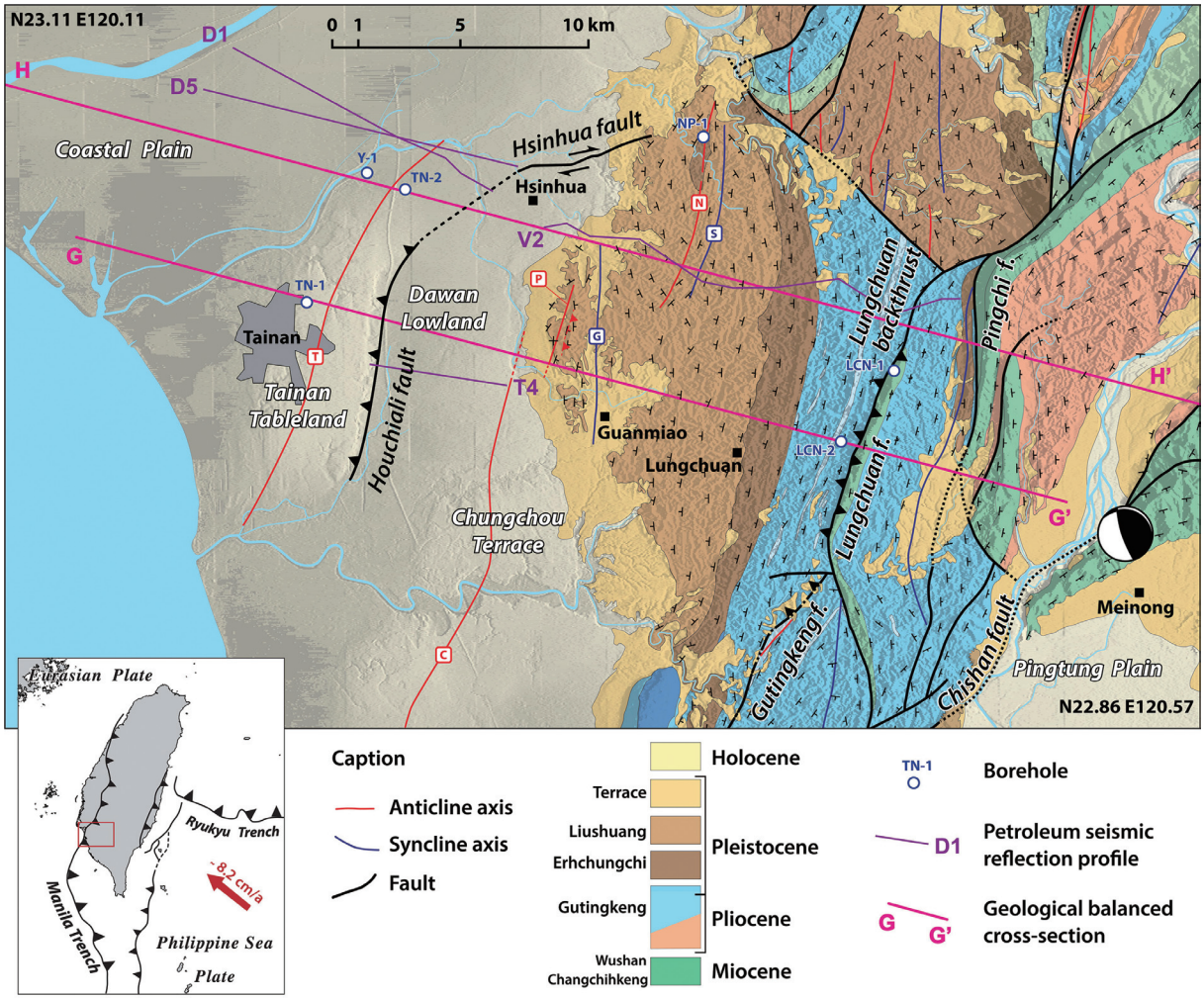

Fig. 1. Regional geologic map of Tainan area, southwestern Taiwan, modified from Chinese Petroleum Corporation 1:100000 map, Tainan sheet (1989). Focal mechanism (Huang et al. 2016a) indicates the Meinong earthquake epicenter. Pink lines = balanced cross-section (this study); Purple lines = petroleum seismic reflection profiles from CPC; White dots = boreholes (see text); Fold axes: T = Tainan anticline, C = Chungchou anticline, P = Pitou anticline, N = Napalin anticline, G = Guanmiao syncline, S = Shihtzuchi syncline. Axes of Tainan and Chungchou anticlines are inferred from Pan (1968) Bouguer gravity anomaly map. Inset map shows the background tectonic setting: Taiwan lies at the convergent boundary between the Luzon volcanic arc on the Philippine Sea plate and the continental margin of the Eurasia plate (Suppe 1984). Present-day plate convergence rate is from Hsu et al. (2009) and Tsai et al. (2015). (Color online only)

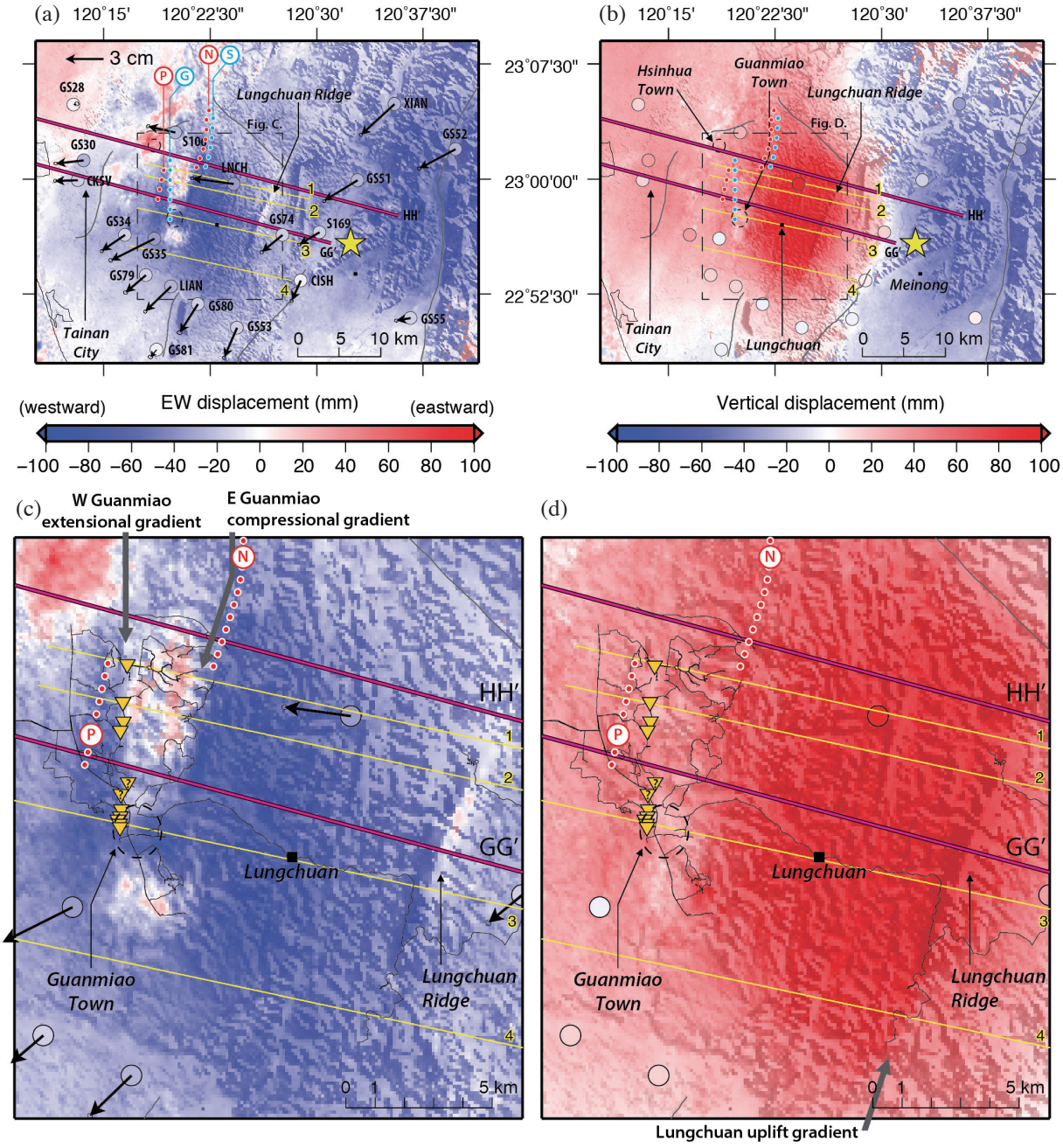

Fig. 2. (a) (b) Overview of east-west and vertical coseismic displacements determined from InSAR on Sentinel-1A images and GPS (black arrows) (Huang et al. 2016a). Yellow star shows the Meinong earthquake epicenter. Black lines are reported active faults from Taiwan Central Geological Survey. Yellow and pink lines correspond to transects shown in Fig. 3 and to geological cross-sections, respectively. Red and blue dotted lines indicate Pitou anticline (P), Guanmiao syncline (G), Napalin anticline (N), and Shihtzuchi syncline (S). (c) (d) Zooms from (a) and (b) on the Guanmiao-Lungchuan area. Yellow triangles show sites where ground surface ruptures were found. Black lines show the path covered during field survey. For convenience, only Pitou and Napalin anticlines are shown. (Color online only)

shallower depth of 5 - 10 km (Huang et al. 2016a). Yet, this model is unable to explain all the details in the observed ground surface deformation, implying that additional structures, probably even shallower, must have been activated during this earthquake.

The foothills of the southwestern Taiwan fold-and-thrust belt accommodate ~4.5 cm yr^{-1} westward shortening (Hsu et al. 2009; Lin et al. 2010; Ching et al. 2011a; Central Geological Survey 2014; Tsai et al. 2015) within ~40 km distance. However, only few active structures have been identified in this area (Central Geological Survey 2010; Shyu et al. 2016) and their geometry and kinematics remain poorly understood. The deformation gradients revealed in InSAR do not correspond to any previously reported active structure.

The aim of this work is to characterize the shallow structures in the foothills of southwestern Taiwan and identify those that could have slipped during or right after the earthquake in order to explain the observed coseismic surface deformation. To do so, we first describe surface deformation based on geodesy and post-earthquake field survey of possible triggered ruptures. Then, we build two new regional E-W balanced cross-sections, based on surface and subsurface geology, as well as crustal deformation during the Meinong earthquake and the interseismic period. Eventually, we combine coseismic deformation and geological structures to infer which structures were or could have been activated during the earthquake and discuss the mechanisms that could have triggered slip on these faults.

2. GROUND SURFACE DEFORMATION

2.1 Overview of Ground Surface Deformation Observed from Geodesy

Coseismic ground surface deformation was observed from InSAR using Sentinel-1A (S1A) and ALOS-2 satellites and GPS. Huang et al. (2016a) used ascending and descending S1A interferograms built with images acquired few days before and ~10 days after the earthquake to decompose the line-of-sight (LOS) displacements into horizontal (mostly E-W) and vertical displacements (Fig. 2). Coseismic displacements at GPS permanent stations were calculated using positions 4 h before and after the earthquake (Huang et al. 2016a).

Northeast and southwest of the epicenter, coseismic displacements are 2 - 3 cm towards southwestern, with slight uplift in the southwestern and slight subsidence in the northeast (Fig. 2). In contrast, 10 - 35 km west of the epicenter, from the Lungchuan ridge area to downtown Tainan, coseismic displacements are oriented mostly westward, with 2.1 - 3.6 cm at GPS stations LNCH, S106, GS30, and CKSV and up to 9 cm from InSAR between Guanmiao town and Lungchuan village. InSAR reveals an area with highest uplift (Fig. 2b) of 8 - 10 cm between Guanmiao and the Lungchuan ridge, with 10.5 cm uplift at GPS station LNCH. On the east side of this area, a significant uplift gradient, oriented N20°E, corresponds to the location of the Lungchuan ridge (Figs. 2 and 3). South of the Lungchuan ridge, the uplift gradient follows the Gutingkeng fault trace and becomes sharper, with an uplift change of ~2.6 cm within a very narrow zone (Fig. 3, Transect 4). The Lungchuan ridge also corresponds to the east edge of a broad zone where westward displacements increase westward. Transects 2 and 3 display a subtle, but sharp increase in westward displacements located at the Lungchuan ridge crest, suggesting slope instability. North and south of Guanmiao, a 10-km-long and 2-3-km-wide area, oriented N5°E to N10°E, is characterized by horizontal displacements close to zero and by smaller uplift (3 - 5 cm) relative to surroundings. On the west side, a sharp extensional displacement gradient is observed along the Guanmiao syncline axis, with an increase in westward displacements of 3 - 5 cm within ~400 m distance westward (strain ~ 10^{-4}) (Fig. 3, Transects 2 and 3). On the east side, ground displacements show a significant compressional gradient, with westward decrease of 7 - 8 cm in westward displacement and of 2 - 4 cm in uplift within 1.0 - 1.5 km (strain ~ -6×10^{-5}) (Fig. 3, Transects 1 and 2). Deformation at Guanmiao town itself appears as an anomaly in this pattern, with a gradient in westward displacement of smaller amplitude (3.5 - 4.0 cm within 0.9 km) that is shifted 1 km to the west compared to north and south of the town (Fig. 3, Transect 3).

2.2 Field Survey of Ground Surface Deformation

2.2.1 Survey Strategy, Limitations, and Methodological Aspects

The relatively sharp deformation gradients revealed by InSAR suggested the possibility of surface ruptures that could bring additional information to understand the geological structures that were activated during the Meinong earthquake. The area between downtown Tainan and the Meinong town exhibited multiple kinds of damage related to various mechanisms: collapsed buildings, damaged buildings and infrastructures, liquefaction features, cracks, small-scale landslides, etc. (Central Geological Survey 2016; Ling-Ho Chung and De-Cheng Yi 2016, personal communication). Because of the limited magnitude of coseismic deformation, offset and aperture along surface ruptures, if any, is expected to be smaller than a few cm. Such features may be hard to distinguish from cracks due to shaking and weaknesses in buildings and infrastructures. Indeed, numerous 1-10-mm-opening tension cracks were found at the tips of bridges, along or across channels, pipes, road ramps and tunnels, and within buildings. The cracks orientation appeared to be guided by the orientation of the infrastructure. Minor tension cracks (< 2 mm opening) and fissures across streets were also nearly ubiquitous within the towns of Guanmiao, Hsinhua, and smaller villages, as well as around major road

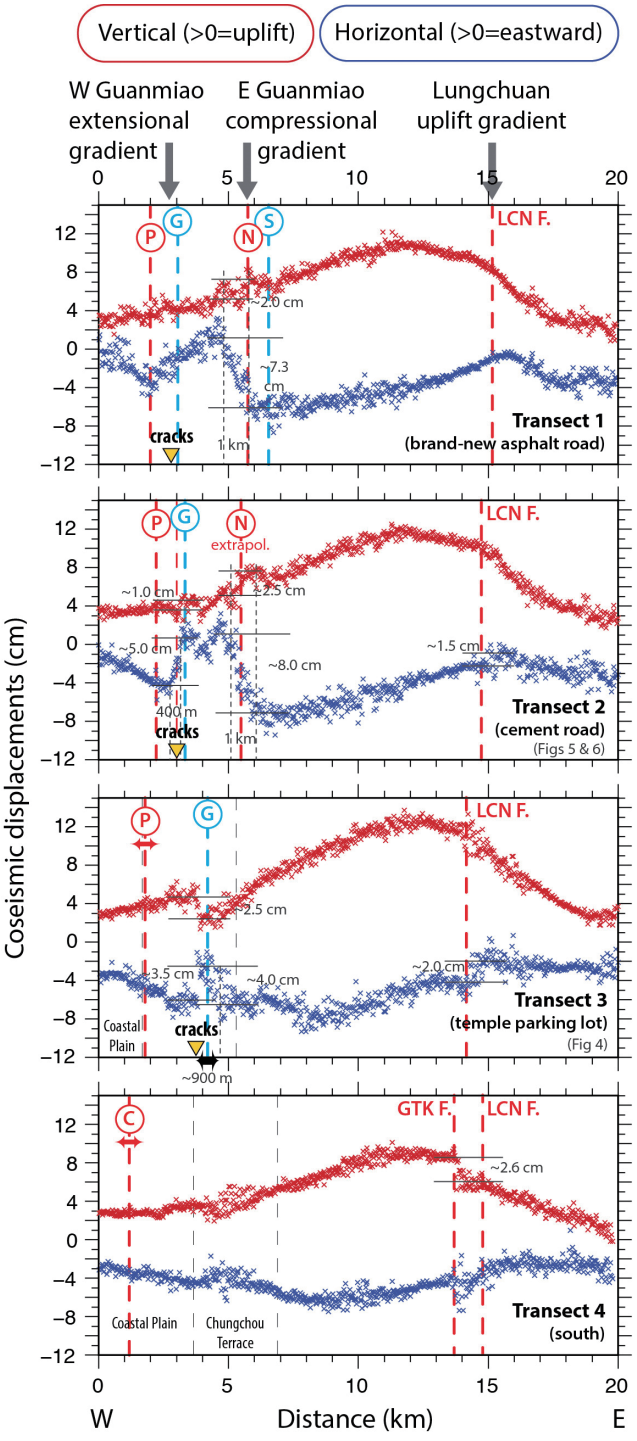

Fig. 3. E-W transects of E-W and vertical coseismic displacements determined from S1A InSAR (Huang et al. 2016a). See location in Fig. 2. P, N, C = Pitou, Napalin, and Chungchou anticlines, G, S = Guanmiao and Shihtzuchi synclines, LCN F. and GTK F. = Lungchuan and Gutingkeng faults (Fig. 1). Black lines and numbers indicate the amplitude and width of displacement gradients. (Color online only)

infrastructures. Although some of these features were located along deformation gradients shown in InSAR (Fig. 2), the remaining cracks were not, questioning the relationship to geological structures. Similar observations, with slightly higher magnitude though, were made in urban areas after the M_w 6.7 1994 Northridge earthquake (Cruikshank et al. 1996; Johnson et al. 1996), the M_w 6.0 2014 South Napa earthquake (GEER Association 2014), and the M_w 6.3 2010 Jia-Shian earthquake (Huang 2013).

To find structurally meaningful cracks corresponding to ground surface ruptures we avoided towns and mainly focused on countryside roads. Careful survey was performed 2 to 7 weeks after the event along significant displacement gradients shown in InSAR, as well as away from them (Fig. 2), as a control of our observations. Guanmiao countryside consists mostly in low hills occupied by fields, farms, forest and grasslands, with lush vegetation, and roamed by tiny asphalt, cement or unpaved roads that we explored on foot or on a scooter at low speed. Cracks location was surveyed using a hand-held GPS with 5 m precision. For series of cracks, the cracks relative position was measured using measuring tape with a precision of 2 - 5 cm. The cracks overall orientation was measured using a compass with a precision of ~2°. Displacement across the cracks was measured using a ruler with a precision of ≤ 0.5 mm. When possible, the slip vector magnitude and orientation were measured using a compass (±1°) and a ruler (±0.5 mm) (Figs. 4 and 5).

2.2.2 Overview of Ground Surface Deformation and Comparison with InSAR Observations

Along the west Guanmiao extensional deformation gradient, sets of significant ~N-S tension cracks were found at multiple places from the center of Guanmiao town until ~5.5 km north (Fig. 2). Similar cracks were found in southwest Guanmiao town (Yi De-Cheng 2016, personal communication), up to 0.7 km south of the southernmost cracks we found. We could not survey deformation further south. The tension cracks usually appear as a set of 2 to 4 main fractures across paved roads, each with ~5 mm opening in the direction ~N80°E to N110°E and distributed over ~25 to ~60 m wide. In addition, they are accompanied with minor tension cracks and fissures, sometimes over a zone up to 300 m wide. The tension cracks did not propagate into the fields on the sides of the road, probably because deformation was small enough to be diffused within soft granular material such as soils. The total displacement cumulated on the sets of cracks is ~1.5 cm of ~E-W extension within ~35 m on the west part of downtown Guanmiao (Fig. 4) and up to ~3.1 cm ~N96°E extension within ~300 m at a countryside road located 4 km north of Guanmiao (Fig. 5). At first order, these values are consistent with E-W displacements observed from InSAR, with 3.0 - 3.5 cm of E-W extension in west Guanmiao and 4.0 - 5.0 cm of E-W extension in the

countryside north of Guanmiao (Fig. 3, Transects 2 and 3). In Guanmiao town, however, no relative vertical displacement was observed across the cracks, while ~2.5 cm uplift of the west block relative to the east block is observed in InSAR. Field measurements are systematically lower than InSAR estimates, probably because deformation may be distributed over a broader area than that covered by paved surfaces. In addition, small deformation accommodated by tilting over a broad area would not be easily identified in the field. At the northernmost site, where the extensional gradient vanishes (Fig. 3, Transect 1), a tension crack with only 2 mm N102°E opening and a minor crack were observed. In areas away from this displacement gradient, only a few tension cracks were found (excluding cracks related to man-made infrastructures other than roads). They consisted in isolated minor cracks or fissures, with any orientation and without meaningful geographic location. To summarize, tension cracks were consistently found along ~5.5 km distance on roads going across the west Guanmiao extensional gradient and displayed extension of the same magnitude, at first order, as InSAR observations. Therefore, we interpret them as a ground surface rupture associated to a geological structure activated during the earthquake. Given the width of the deformation zone, ground surface deformation likely reflects an active hinge zone or a buried fault (Huang and Johnson 2010).

The east Guanmiao compressional deformation gradient was also surveyed in detail (Fig. 2). However, only isolated minor tension cracks with random location were found. This displacement gradient could be too gentle to result in recognizable deformation in the field (maximum 8 cm over 1 km; Fig. 3), and the displacement is possibly

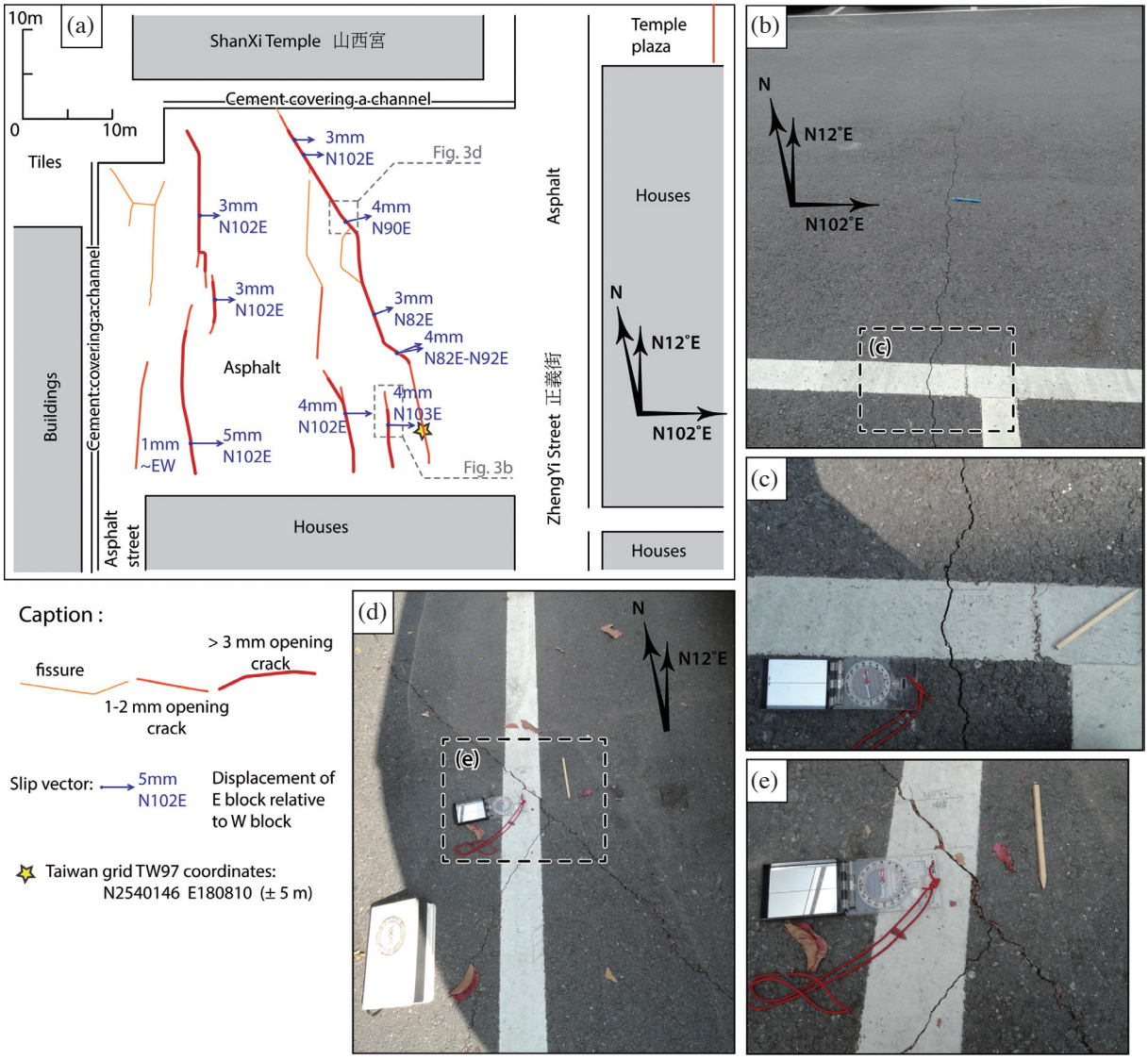

Fig. 4. Tension cracks on a temple parking lot in Guanmiao town: (a) Sketch map, (b) to (e): Field photographs of major cracks where slip vectors could be measured. Site is located along Transect 3 of Figs. 2 and 3. (Color online only)

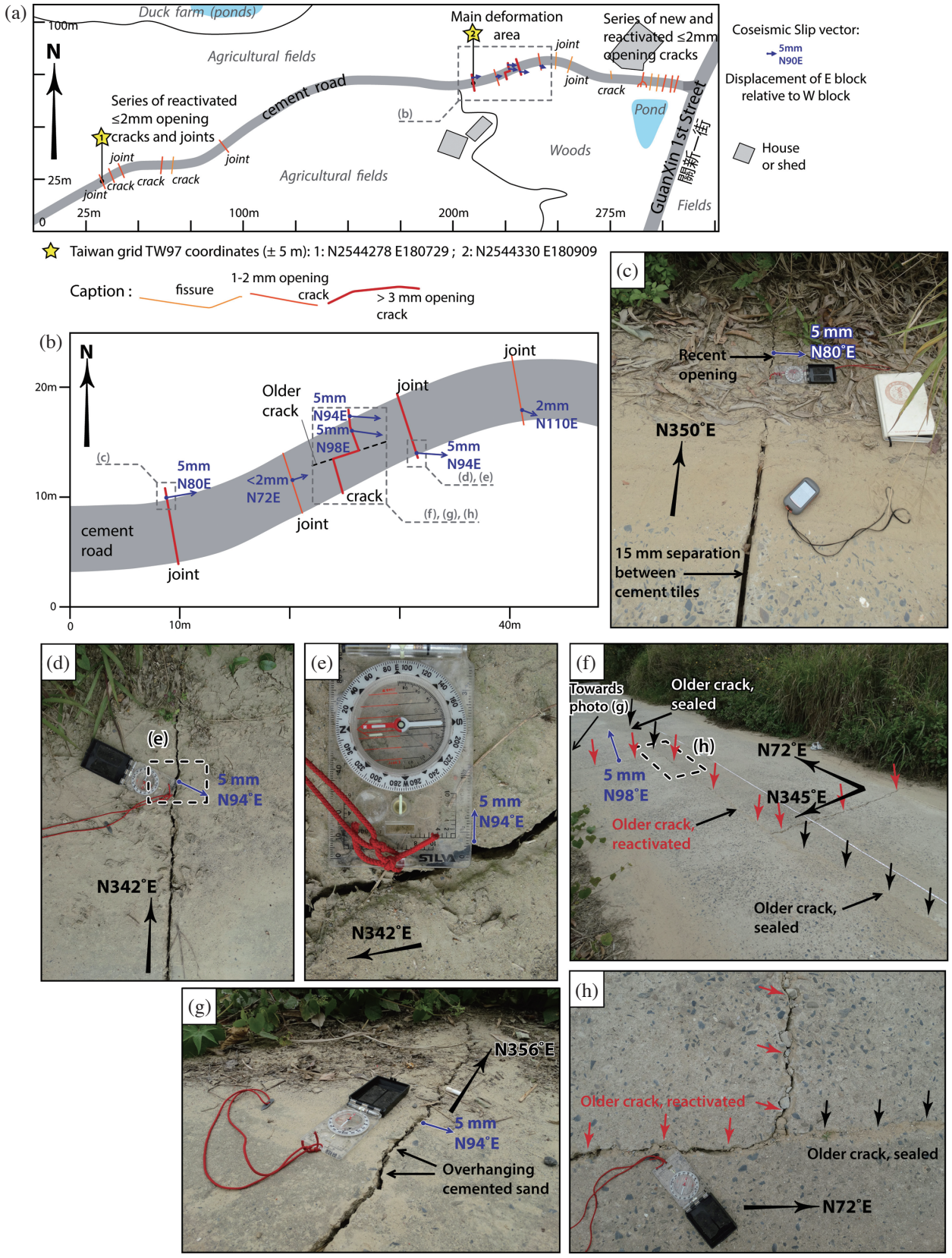

Fig. 5. (a) (b) Sketch maps of tension cracks along a countryside road located 4.0 km north of Guanmiao town and made of 10-m-long cement tiles. Panel (b) focuses on the most significant cracks. Site is located along Transect 2 of Figs. 2 and 3. (c) - (h) Field photographs of the main tension cracks found. See locations on (a) and (b). (Color online only)

related to tilting of the ground surface.

Along the Lungchuan ridge, only a quick survey using a car was done across the north and south tips of the ridge (Fig. 2). However, no obvious localized ground deformation (> 5 mm amplitude) could be observed.

2.3 Tension Cracks Along the West Guanmiao Extensional Deformation Gradient

In this section, we describe in more details the tension cracks observed at two locations along the west Guanmiao extensional gradient. In western Guanmiao town, a set of ~N-S tension cracks could be observed more extensively on a temple parking lot recently paved with asphalt (Fig. 4). There, we observed a network of 2 to 3 main tension cracks, oriented N350°E to N12°E and a few minor cracks and fissures. The cracks sharp and distinctive edges provided good markers that allowed measuring slip vectors, oriented N82°E to N103°E with displacements of 3 to 5 mm of the east blocks away from the west blocks. The total extension across this set of cracks is 16 mm in the direction N102°E at the south edge of the parking lot, decreasing to 6 mm in the direction N102°E at the north edge. North of the parking lot, the temple does not exhibit any damage of the pavement nor the walls, probably due to the building strength.

Four km north of downtown Guanmiao, along a road made of ~10-m-long cement tiles, we observed a set of 19 road-perpendicular fractures, including tension cracks, opened joints between cement tiles, and fissures (Fig. 5). On the west part of the site, we found a set of 5 open joints and tension cracks within ~65 m, oriented N337°E to N6°E. The cracks were reactivated from older cracks, but it is hard to conclude if the joints were opened during the earthquake, as the tiles may not have been perfectly adjusted to each other when the road was built. Recent opening of 1 - 2 mm for each crack and joint is evidenced from sharp cracks within the fine sand that fills the fractures and from a break in the dirt covering the vertical edge of the road. About 100 m further east, a set of 5 open joints and tension crack showed more significant deformation. The central part of the joints, oriented N342°E to N350°E, displayed total separation up to 15 mm, which may result from poor tiles adjustment during road construction and from any subsequent displacements. However, the roadsides were covered with slightly cemented fine sand and silt, displaying recent fractures of smaller aperture (Figs. 5c, d, e). The cracks exhibit sharp irregular edges with pieces of cemented sand overhanging above the cracks. Because these micro-overhangs could have been destroyed by rain or any other source of disturbance, they are strong evidence of very recent deformation. The irregular edges of the cracked sand cover lead to slip vectors of 5 mm along N80°E, < 2 mm along N72°E, 5 mm along N94°E, and 2 mm along N110°E (Fig. 5). This site includes a peculiar Z-shape crack (Figs. 5f, g, h), composed of 2 road-perpendicular segments, oriented N339°E to N356°E, connected by a third segment, N72°E, that was reactivated from an older crack visible in the central part of the road. Recent deformation could be confidently measured only along the north crack segment: 5 mm along N94°E to N98°E. About 50 m further east, a set of 6 new and reactivated tension cracks, oriented N8°E to N15°E, displayed ≤ 2-mm crack-perpendicular (N98°E to N105°E) opening. Total extension across the whole site is 31 mm, half of it distributed on 3 open joints and tension crack. The slip vectors average orientation is N96°E ± 11°.

3. GEOLOGICAL STRUCTURES IN THE COASTAL PLAIN AND WESTERN FOOTHILLS OF TAINAN REGION

3.1 Surface and Subsurface Geological Data and Kinematic Constraints

Strike and dip data from surface geology come from the 1:100000 geological map of Tainan (Chinese Petroleum Corporation 1989) and from an unpublished local geological map (scale 1:25000) in the Lungchuan ridge area (Yu et al. 1990), complemented by our own structural measurements in Guanmiao area. We benefit from petroleum seismic reflection profiles D1, D5, V2, and T4 (Figs. 1 and 6), with depth conversion performed on lines D1 and D5 (Marc et al. 2010). Additional subsurface constraints come from boreholes TN-1, TN-2, and LCN-2 (Huang et al. 2004), NP-1 (Chung 1968), Y-1, and LCN-1.

We also used coseismic displacements during the Meinong earthquake (InSAR and GPS; Huang et al. 2016a) and interseismic crustal deformation data in order to locate areas where uplift occurs and shortening is consumed (Figs. 7 and 8). Interseismic velocities come from campaign GPS network from Taiwan Central Geological Survey (e.g., Ching et al. 2011a; Central Geological Survey 2014) during 2002 - 2014, from precise leveling (e.g., Ching et al. 2011b; Central Geological Survey 2014) during 2012 - 2015, and from linear regression through position time series of permanent GPS stations of the Institute of Earth Sciences, Academia Sinica, network (e.g., Tsai et al. 2015). Interseismic deformation was also monitored from InSAR using 13 images from the ALOS-1 satellite acquired during the period 2007 - 2010 (before the 2010 Jia-Shian earthquake; e.g., Huang et al. 2013), along an ascending path, with radar line of sight toward the east with an incidence angle of ~40° (Pathier et al. 2014). Interseismic LOS displacements are derived from a time-series analysis based on a small baseline approach (NSBAS method, Doin et al. 2011), including atmospheric correction using European Centre for Median-Range Weather Forecast ERAI reanalysis (Doin et al. 2009; Jolivet et al. 2011), DEM errors correction performed before unwrapping (Ducret et al. 2014), and unwrapping following a method similar to Grandin et al. (2012).

3.2 Structural Elements in the Study Area

3.2.1 Within the Coastal Plain

The subsurface structure of Tainan anticline has been previously investigated thanks to depth-converted seismic lines D1 and D5 located at the anticline north tip (Fig. 1), combined with InSAR observations and geomorphic analysis. The gently folded reflectors were interpreted as a pure-shear wedge fault-bend-fold growing above a backthrust that corresponds to the Houchiali fault. The backthrust roots on a detachment, the Tainan detachment, at a depth of ~3.6 km that was constrained from the deepest deformed reflectors (Marc et al. 2010) and corresponds to the Pliocene Lower Gutingkeng mudstone (Fig. 7c). The analysis of InSAR LOS velocities during the aseismic slip period of 1996 - 1999 (Fruneau et al. 2001; Huang et al. 2009, 2016b) shows that the surface deformation at the Tainan Tableland is consistent with the structural model proposed from the seismic lines north of the tableland (Le Béon et al. 2014). Therefore, a similar pure-shear wedge fault-bend fold model may apply to the Tainan anticline, with a backthrust that may be steeper along the tableland compared to north of it. The cumulative shortening along the seismic lines was determined to ~800 m only (Marc et al. 2010). The more pronounced topographic expression of the fold to the south and the shallower depth of stratigraphic horizons in borehole TN-1 compared to borehole TN-2 (Fig. 1; Huang et al. 2004) show that cumulative shortening must be larger to the south. To expand the balanced cross-sections to the east, we use the detachment depth of ~3.6 km and a regional dip for the detachment of 2°E to account for the geometry of the Chinese continental shelf.

3.2.2 At the Toe of the Western Foothills

On seismic reflection profile V2 (Figs. 1 and 6), continuous reflectors from the west tip to ~6 km distance show an asymmetric anticline, the Napalin anticline, with a steep and narrow east limb, corresponding to 28 - 50°E dips in the surface geology, and a wide west limb with shallower dips, consistent with surface geology (10 - 20°W). Dip angles appear to be similar for the deeper reflectors of the west limb and become progressively shallower towards the surface within the Pleistocene Liushuang formation, indicative of syntectonic sedimentation above a fold limb that grows by limb rotation (Suppe et al. 2004; Shaw et al. 2005). The deeper reflectors were tentatively mapped as the Pleistocene Erhchungchi formation since it crops out along the Napalin anticline 3 km north of V2 (Fig. 1). At ~6 km distance along V2, reflectors are poorly imaged, impeding to conclude on the exact structure of the east limb. The seismic line displays continuous reflectors again from ~6 to ~11 km with increasing west dips towards the east across 2 axial surfaces, and is in agreement with surface geology. Within each kink band, dip angles appear to be similar to each other. The reflection quality drops at the contact between the Erhchungchi formation and the Gutingkeng mudstone.

Because the Napalin anticline is an east-verging fold with the west limb growing by limb rotation, we propose a detachment fold (Epard and Groshong 1995) or a pure-shear fault-related fold (Suppe et al. 2004) growing above a backthrust, such as a fault-propagation fold (Suppe and Medwedeff 1990) or a tri-shear fold (Hardy and Allmendinger 2009). Because the thickness of sediments displaying

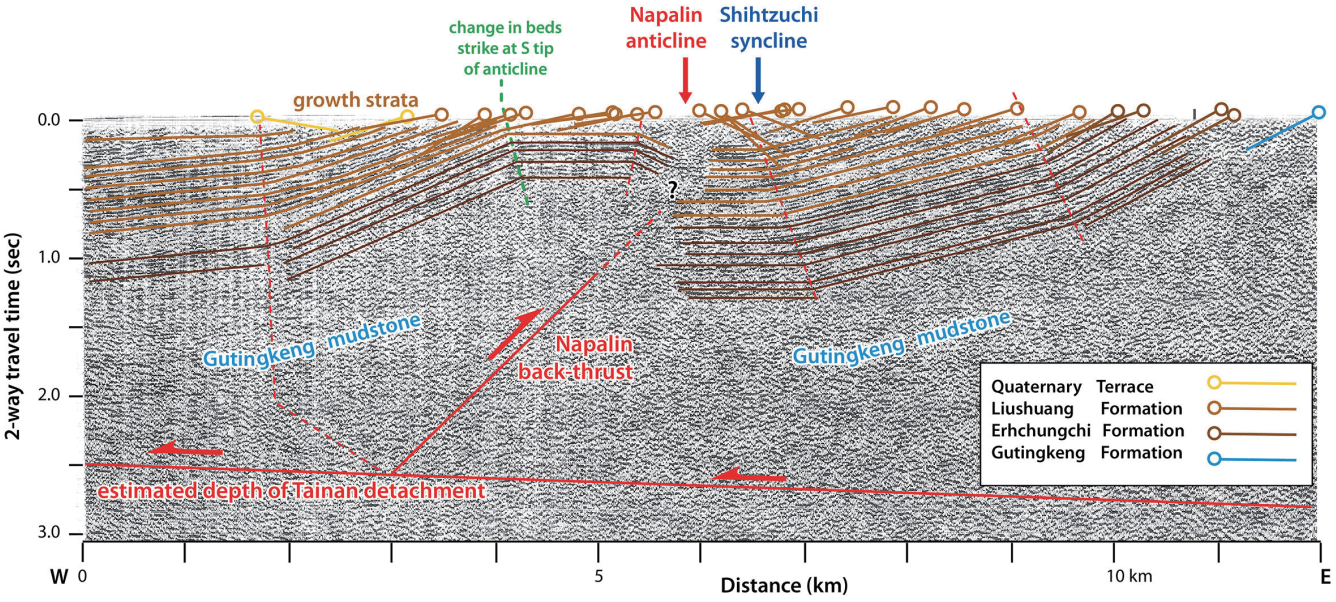

Fig. 6. Interpretation of petroleum seismic reflection profile V2 (location on Fig. 1) across the Napalin anticline, based on unmapped profile Sa1 published in Huang et al. (2004). Green dotted line correspond to an apparent hinge due to changes in bedding strike and in seismic line orientation (Fig. 1). (Color online only)

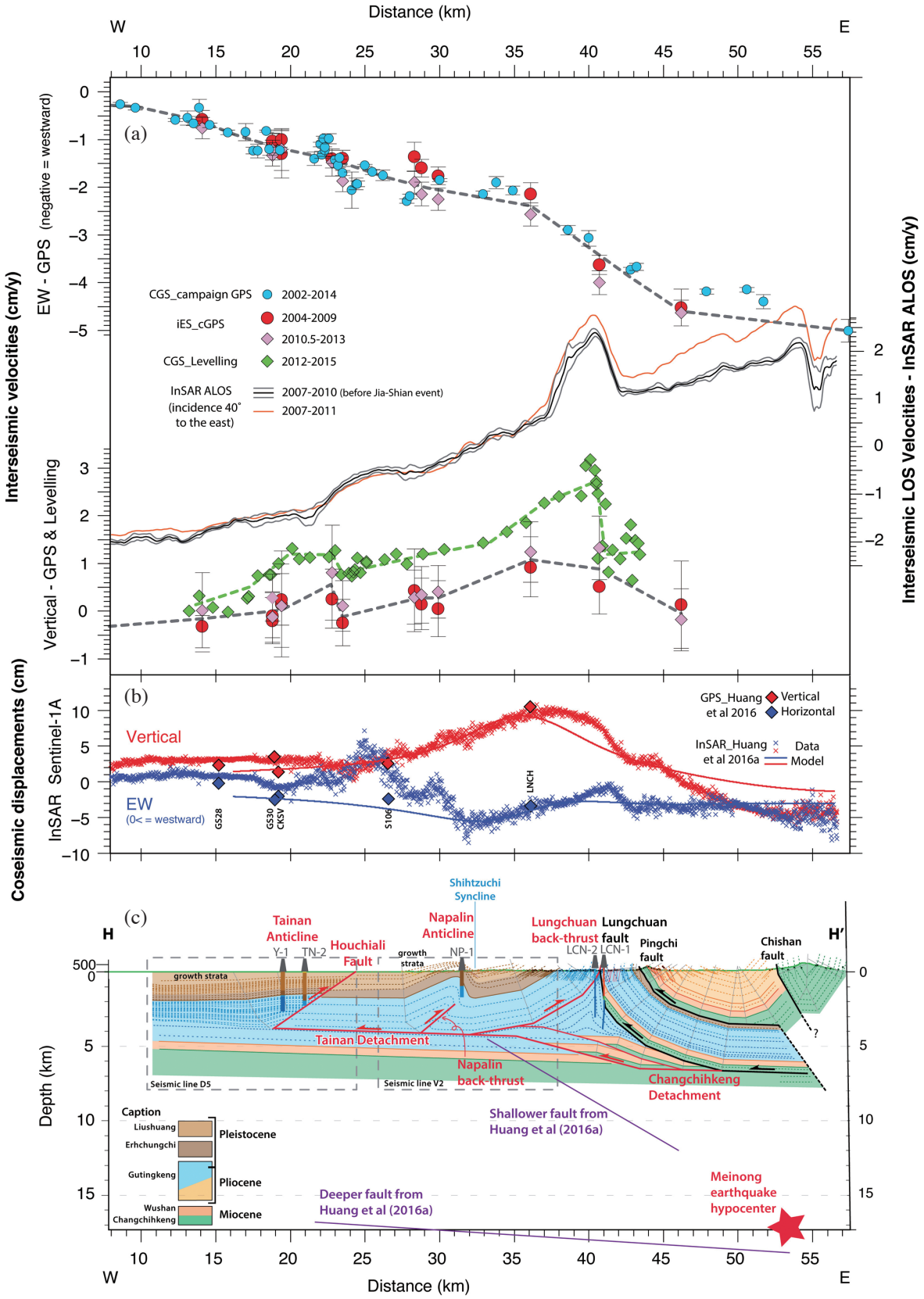

Fig. 7. Transect HH' (Fig. 1): (a) Interseismic GPS, levelling and InSAR ALOS-1 line-of-sight velocities (Central Geological Survey 2014; Pathier et al. 2014). (b) Meinong coseismic E-W and vertical displacements based on Huang et al. (2016a) dataset. (c) Balanced geological cross-section. Red faults are inferred to have activated during the Meinong earthquake. The earthquake hypocenter is indicated for reference, as well as the deep and shallower faults inferred by Huang et al. (2016a) (Purple lines). Note that the shallow dip of Huang et al deep fault (N61°W, dip 15°NE) is apparent. (Color online only)

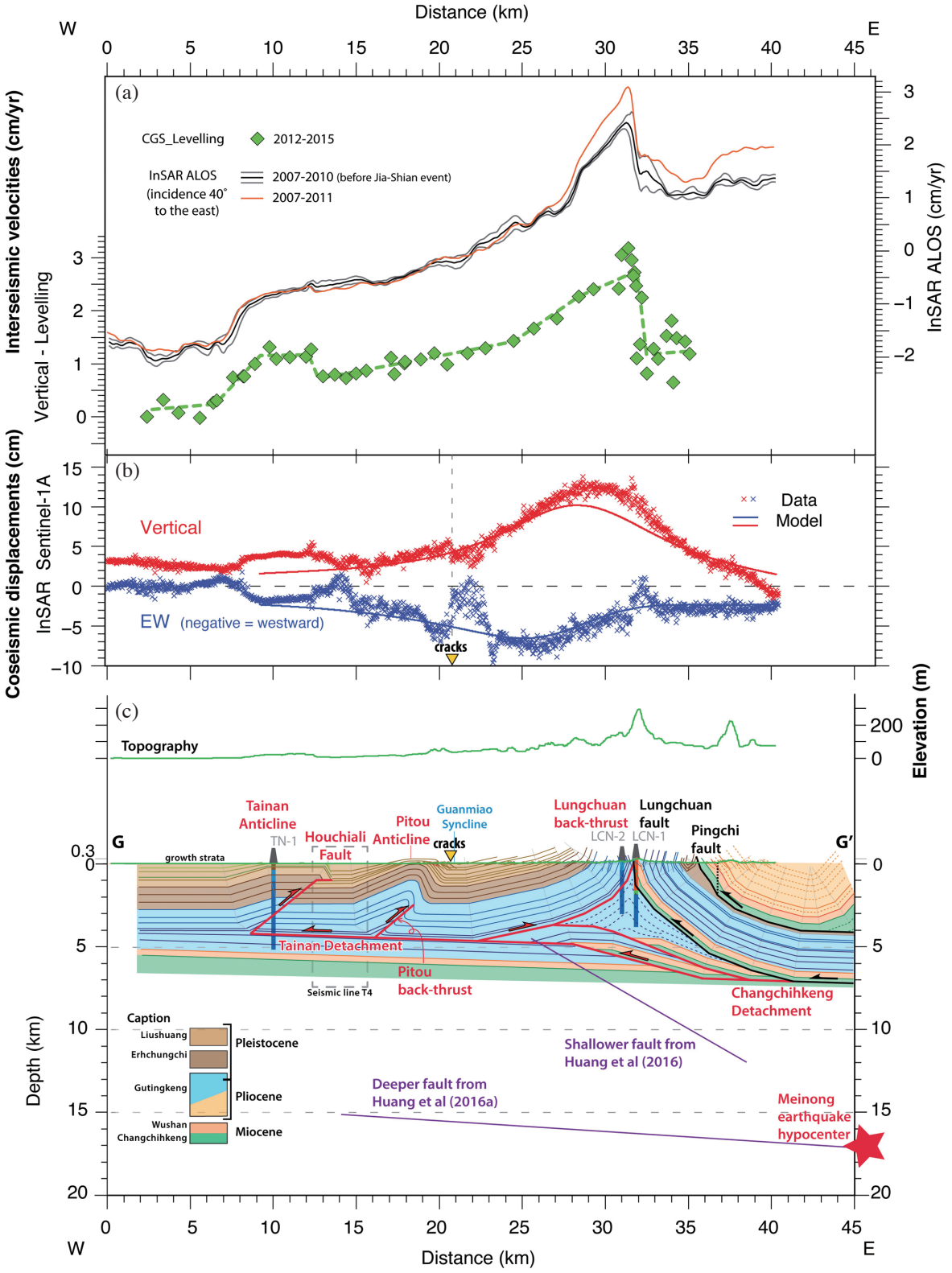

Fig. 8. Transect GG' (Fig. 1): (a) Interseismic leveling data and InSAR ALOS-1 line-of-sight velocities (Central Geological Survey 2014; Pathier et al. 2014). (b) Meinong coseismic E-W and vertical displacements (Huang et al. 2016a). (c) Balanced geological cross-section. Red faults are inferred to have activated during the Meinong earthquake. Green line above section shows exaggerated topography. (Color online only)

good reflection properties is very different across a fairly narrow zone (~1 km) and also because the east-dipping beds in the surface geology are located above the subhorizontal reflectors at depth (Fig. 6), we favor a tri-shear fold, with a west limb growing by limb rotation. In cross-section HH', the limited width of the fold compared to the detachment depth requires a fairly steep dip of 37° for the backthrust (Fig. 7c). We called this backthrust the Napalin backthrust. We cannot exclude the alternative possibility that the fault reaches the surface.

The toe of the Foothills at the latitude of section GG' seems to consist in similar structures, but they are partially imaged. In spite of lower quality imaging, seismic line T4 displays subhorizontal reflectors down to at least 2.5 s from the Houchiali fault trace to 2.5 km to the east. Then, from 2.5 - 3.0 km east of the Houchiali fault trace, the reflectors show west dips down to 2.0 s. Further east, no reflector is imaged in the seismic line. Four km further east, between Guanmiao and Hsinhua towns, surface geology shows an anticline, that we called the Pitou anticline (Figs. 1 and 8c), with shallow west dips of 2 - 9° on the west limb and a narrow and steep (28 - 43°E dips) east limb, similarly to the Napalin anticline east limb. As a simple structural interpretation, we propose that the west dips observed on T4 in Dawan Lowland and at the toe of the foothills connect to each other, which results in a 5-km wide shallow fold limb, similar to the west limb of Napalin anticline (Fig. 8c). East of the Pitou anticline, surface geology shows a syncline axis, the Guanmiao syncline, and shallow west-dipping beds, with dip increasing to the east, similarly to section HH' (Figs. 1, 7c, 8c). Therefore, the Pitou anticline and Guanmiao syncline, on one hand, and the Napalin anticline and Shihtzuchi syncline, on the other hand, appear to be similar en-echelon structures (Fig. 1). Therefore, similarly to the Napalin anticline, we expect the Pitou anticline to grow above a backthrust, that we refer to as the Pitou backthrust. Based on Bouguer gravity anomalies (Pan 1968), these anticlines likely correspond to the northern continuation of the Chungchou anticline, possibly en echelon to the west relative to the Pitou anticline (Fig. 1).

3.2.3 In the Lungchuan Ridge Area

Constraints to build this part of the cross-sections come from surface geology, boreholes, and crustal deformation. On one hand, surface geology east of the Lungchuan ridge and borehole LCN-1 show that the Miocene Wushan sandstone that forms the ridge has been brought to the surface by an east-dipping thrust fault reaching the surface at the west toe of the ridge (Figs. 7c and 8c). Surface geology and borehole data constrain the Lungchuan fault to be subvertical from the surface down to 2.0 - 2.5 km depth, questioning how such fault could be activated as a thrust in the present day. On the other hand, precise leveling and InSAR during the interseismic period show sharp uplift and LOS deformation gradients at the Lungchuan fault trace and Gutingkeng fault trace, with the west side going up relative to the east side (Figs. 7a and 8a). Moving west from the Lungchuan fault, leveling shows constant or slightly westward decreasing uplift over ~3 km, then a sharper westward decrease in uplift over ~4 km, to reach a gentle westward decrease until the Houchiali fault ~10 km further west. The sharpness of the displacement gradient strongly suggests the presence of a fault reaching the surface and likely creeping. This higher uplift area is also associated with a higher gradient in E-W shortening shown by GPS (Fig. 7a). These observations are inconsistent with tectonic activity on the east-dipping Lungchuan fault. However, they could be explained by a backthrust within the Lower Gutingkeng formation and reaching the surface west of the Lungchuan ridge, possibly at the same location as the east-dipping Lungchuan fault. South of the Lungchuan ridge, the backthrust would follow the trace of the Gutingkeng fault. The existence of this backthrust was previously proposed in Huang et al. (2004) as well. We call this backthrust the Lungchuan backthrust. The sedimentary thickness on the hanging wall of the backthrust is closely similar to the sedimentary thickness in the Coastal Plain, supporting this interpretation. If simply propagating surface dips to depth, the backthrust consistently flattens at a depth similar to the Tainan detachment, also validating a regional dip of 2°E for the Mio-Pliocene sediments.

In borehole LCN-1, the Miocene Changchihkeng formation has been reported on top of the Plio-Pleistocene Gutingkeng formation (Fig. 7c). Thus, the Lungchuan fault must ramp up from a detachment within the Changchihkeng formation, i.e., deeper than the Tainan detachment. Therefore, a ramp from the Changchihkeng detachment to the Lower Gutingkeng detachment must be located somewhere beneath the Lungchuan ridge area, at depths of 5 to 7 km.

A vast triangular space remains between the detachment levels, the Lungchuan fault and the Lungchuan backthrust, with a narrowly pinched upper corner. Boreholes LCN-1 and LCN-2 show that this volume is filled with Gutingkeng mudstone down to 4.2 km depth. Borehole dip data, as reliable as they could be in such homogeneous and low-rigidity rock formation, show fairly consistent dip values of 48 to 60°, on either direction. The available space between 4.5 and 7 km depth can be fitted reasonably well with 2 ramps, imbricated under the Lungchuan thrust sheet (Suppe 1980), involving mainly resistant Changchichkeng and Wushan formations. We propose that the upper part of the triangle consists in Gutingkeng sediments that have been detached from the Wushan sandstone under the stress generated by thrusting of the Lungchuan thrust sheet. This could have been permitted by the high contrast in mechanical properties between the strong Wushan sandstone and Changchihkeng formation, acting as an indenter, and the soft plastic mudstone of Gutingkeng formation, resulting in a narrow detachment fold.

4. DISCUSSION

4.1 Geological Structures Activated During the Meinong Earthquake

4.1.1 Activation of the Ramp and Comparison with the Shallower Fault Inferred from Modeling of Geodetic Data

Following earthquake source modeling of Huang et al. (2016a) based on joint inversion of seismic waveforms and geodetic data, we included for reference the location of the deeper fault where the earthquake nucleated and of the shallower fault on the cross-sections (Figs. 7c and 8c). The shallower fault strikes N8°E, dips 30°E and ranges from 4.5 to 12 km depth, with most slip between 6 and 9 km depth. Interestingly, it is located at very similar distances along the cross-sections to the ramps inferred independently from geology with, however, a deeper depth range than the 5 to 7 km depth of the geology-based ramp and a steeper dip angle (15° for the geology-based ramp). For kinematic dislocation inversions, the inferred fault depth or the amount of fault slip is highly dependent of the geodetic data accuracy, as well as of the assumed layered structure computed for Green's functions (Hearn and Bürgmann 2005). More importantly, due to high fluid pressure inferred from the high Vp/Vs ratio underneath the region between Guanmiao and Lungchuan (Huang et al. 2016a), the coseismic deformation at shallower depth here may be inelastic. If we account for inelastic (e.g., plastic) deformation component in the kinematic fault modeling, the inferred fault depth could be shallower. Similarly, the ramps inferred from geology lack precise constraints and could bear a little different attitude. Nonetheless, it seems very likely that the shallower fault inferred by Huang et al. (2016a) could correspond to a ramp at first order similar to the one on cross-sections HH' and GG'. Therefore, this ramp was likely activated during the Meinong earthquake, allowing potential input of westward slip on the Tainan detachment and shallower backthrusts that root on this detachment.

4.1.2 The Lungchuan Backthrust

The Lungchuan backthrust is the easternmost structure that roots on the Tainan detachment. Based on InSAR and our field exploration, it is not clear if this fault produced surface rupture. Only Transect 4 (Fig. 3) shows a displacement discontinuity across the backthrust that suggests fault slip had reached the surface. Yet, the overall shape of the coseismic uplift transects based on InSAR shows a similar pattern to the leveling transect during the interseismic period, with a gentle eastward increase in uplift, and then a sharp decrease in uplift that corresponds to the Lungchuan backthrust surface trace. This asymmetry is not predicted in Huang et al. (2016a) model (Figs. 7b and 8b), because they did not attempt to model the shallowest fault slip. A contribution to deformation from the Lungchuan backthrust would produce such east-verging uplift pattern. Therefore, the earthquake likely activated the Lungchuan backthrust. Regarding uplift budget, since the geology-based ramp is shallower than the model ramp of Huang et al. (2016a), the deficit in uplift due to a shallower ramp may be compensated by slip on the Lungchuan backthrust.

4.1.3 Extensional and Compressional Gradients Within the Foothills

Along cross-section HH' (Fig. 7), the east Guanmiao compressional gradient corresponds to the steep east limb of Napalin anticline, which we proposed to grow above the buried Napalin backthrust. Activation of this backthrust would be consistent with consumption of E-W shortening at the anticline east limb. However, while the Napalin anticline is visible in the surface geology until > 6 km further north of HH', the compressional gradient vanishes only 2 - 3 km north of HH' (Figs. 1 and 2). In contrast, the Napalin anticline is not observed 1.5 km south of HH', while the compressional gradient is observed until 10 km south. These observations do not favor the Napalin backthrust as the origin of this deformation gradient. South of HH', the east Guanmiao compressional gradient does not correspond to any change in the surface geology, which consists in shallow ~12°W dips over a broad area. At greater depth, however, it corresponds, for both sections HH' and GG', to the tip of the wedge between the ramp and the Lungchuan backthrust, that we argued to have been active during the earthquake. Because of the consistency of surface geology from HH' until ~12 km further south (Fig. 1), this deep structure is expected to exist everywhere beneath the east Guanmiao compressional gradient, so that it appears to be a good candidate to explain this compressional gradient. To get such compression, a significant part of the slip on the ramp must be transferred to the Lungchuan backthrust, while only a smaller portion propagates westward on the Tainan detachment. As mentioned in section 2.1, at Guanmiao town the east Guanmiao compressional gradient is shifted 1 km to the west compared to north and south of the town (Fig. 3, Transect 3). It is very unlikely that geological structures differ beneath Guanmiao town, thus we hypothesize that this shift may be due to a different response of the ground surface in Guanmiao town. The town is densely covered with paved roads and buildings that may make it more resistant to such small deformation, while the surroundings consist in agricultural lands and forest that behave more like a free surface.

Along cross-section GG', ~4.0 cm E-W extension is observed across the west Guanmiao extensional gradient, where tension cracks were observed in the field (Fig. 2, Transect 2; Fig. 8b). It corresponds to the surface trace of the Guanmiao syncline, i.e., the extrapolated trace of the Pitou backthrust in our interpretation (Fig. 8c). Along section HH',

extension is very subtle, only ~1.0 cm and no surface cracks were found at this latitude (Figs. 2 and 7b). This deformation is still likely related to the Pitou-Guanmiao structure that ends only a few 100 m south. E-W extension is however inconsistent with a backthrust, as well as with a syncline axis and the regional tectonic setting. Instead, this extension may be transient deformation such as elastic pull towards east due to the activation of another nearby structure, which likely is the Lungchuan backthrust. The steep east limb of the Pitou anticline, that we argued to be controlled by the buried Pitou backthrust, represents a significant change in the geological structure or a significant weakness zone that could accommodate this eastward elastic pull.

West of the extensional gradient, the Pitou anticline shows absolute westward motion again and higher uplift relative to Guanmiao area (Figs. 2 and 8b). Such displacements may be explained by slip on the deeper fault based on Huang et al. (2016a) model. It is also possible that the Pitou backthrust was activated by slip on the Tainan detachment and/or potentially promoted by a decrease in normal stress due to local extension.

4.1.4 The Houchiali Fault and the Hsinhua Fault

The InSAR and GPS coseismic displacements (Figs. 2, 7b, and 8b) show ~2 cm uplift and westward displacements on Tainan Tableland relative to the Coastal Plain and Dawan Lowland. It indicates a minor reactivation of the Houchiali fault and also implies that the Tainan detachment may have slipped as far west as downtown Tainan City during or shortly after the Meinong earthquake.

The ~N70°E Hsinhua fault is surrounded by a complex surface deformation field (Figs. 1 and 2), with patches of eastward displacements on the west part and patches of westward displacements on the east part. The overall orientation of these displacement patches is ~N20°E, subparallel to strike-and-dip data at the toe of the foothills and highly oblique to the Hsinhua fault trace, which was highlighted by liquefaction features during the earthquake (Central Geological Survey 2016). The right-lateral Hsinhua fault slipped during the M 6.4 earthquake in 1946 (Bonilla 1975) and appears to act as a tear fault from the toe of the foothills to the Houchiali fault and Tainan anticline. Its role during the Meinong earthquake may have been limited to a weak zone through which over-pressured fluids found their way to the ground surface.

4.2 Relationship to the Earthquake Source and Trigger Mechanism

The shallow structures that activated during the Meinong earthquake are located 10 to 35 km west of the hypocenter and at >10-km shallower depth (Figs. 7c and 8c), raising the question of the structural or mechanical connections between faults and earthquake source. Huang et al. (2016a) highlighted that the static Coulomb stress change due to slip on their inferred deeper fault did not promote slip of the shallower fault. The depth and dip angle of the ramp inferred in this study are slightly different from the shallower fault inferred in Huang et al. (2016a), but the difference may not be significant enough to switch the static Coulomb stress change to fault failure. We cannot rule out, however, the existence of other structures between the hypocenter and the shallow structures, such as deeper detachment(s) or possible reactivated Paleogene normal faults (e.g., Mouthereau et al. 2001; Carena et al 2002; Mouthereau and Lacombe 2006; Rodriguez-Roa and Wiltschko 2010; Camanni et al. 2016), that could have promoted slip on the shallower ramp. Alternatively, these shallow structures could be activated dynamically by seismic waves radiated from the Meinong main fault structure (e.g., Freed 2005).

Earthquake source models based on seismic waveforms converge to a slip patch restricted to the main deep fault close to the epicenter (Lee et al. 2016; Kanamori et al. 2017; Wen et al. 2017). Consequently, the shallow faults that slipped beneath the Guanmiao-Lungchuan area did not contribute to seismic waves radiation, so that slip is inferred to be slow or aseismic. High-rate GPS (1 Hz) shows that surface deformation in the Guanmiao-Lungchuan area occurred within 20 seconds after the main shock (Tung et al. 2016), so that this aseismic event, which would be equivalent to a M ~5.7 - 5.9 earthquake (Huang et al. 2016a), occurred coseismically.

The foothills of southwestern Taiwan showed cases of aseismic slip prior to the Meinong earthquake, both during interseismic periods and during co- and post-seismic periods. The most obvious example is the creeping Chishan fault that has been progressively deforming a tunnel along National Highway 3, ~18 km south of GPS station LNCH (Central Geological Survey 2014). Within our study area, the sharp gradients in uplift based on leveling and in LOS deformation based on InSAR (Fig. 7a) also suggest that the Lungchuan backthrust was creeping during the interseismic period before the Meinong earthquake. Based on InSAR studies, transient aseismic slip on the Houchali fault was also inferred during the period 1996 - 1999 (Huang et al. 2006, 2009) and during 2005 - 2008 (Huang et al. 2016b). In addition, increased deformation rates across the Houchiali fault were reported during the observation time window that included the 1999 M_w 7.6 Chi-Chi earthquake that occurred ~110 km to the northeast (Kao and Chen 2000). Last but not least, the M_w 6.3 2010 Jia-Shian earthquake located ~20 km east of Meinong town may have activated the Lungchuan backthrust and likely other structures (Huang et al. 2013; Lin et al. 2015). The focal mechanism and nucleation depth of the Jia-Shian event are very similar to the Meinong event. Similarly to the Meinong event, seismic waves radiated mainly from a deep slip patch close to the hypocenter

(Ching et al. 2011c; Hsu et al. 2011; Huang et al. 2013; Lin et al. 2015). It generated minor cracks around Meinong town (Huang 2013). ALOS InSAR results show 2 - 5 cm LOS displacements on the hanging wall of the Lungchuan backthrust during a time period covering Jia-Shian earthquake and the following 4 months (Huang et al. 2013). Similarly, longer-term ALOS InSAR observations of interseismic deformation (Pathier et al. 2014) also captured larger velocities on the hanging wall of the Lungchuan backthrust during the period 2007 - 2011 compared to 2007 - 2010 that does not include the Jia-Shian event (Figs. 7a and 8a). The continuous GPS stations maintained by the Institute of Earth Science at Academia Sinica show up to ~5 cm total uplift in Lungchuan, Guanmiao, and Hsinhua area several weeks after the Jia-Shian earthquake, whereas no significant coseismic vertical displacement was observed at these stations. Note that the post-earthquake GPS velocities at these continuous stations are slightly higher after the Jia-Shian event (starting 4 months after the event) compared to before the event (Fig. 7a). This was only recorded for the stations near the Guanmiao-Lungchuan area. The GPS data from stations closer to the Jia-Shian epicenter do not show a significant increase of vertical velocity. We therefore infer that the 2010 Jia-Shian earthquake has temporally increased the slip rate on the shallow structures in the Guanmiao-Lungchuan region.

Long-distance triggering had been observed along the creeping segments of the south San Andreas Fault System after several moderate to large earthquakes (Allen et al. 1972; Bodin et al. 1994), developing the idea that creeping faults can be easily triggered by the passage of seismic waves. Numerical modeling (Du et al. 2003) later supported this hypothesis. The faults mentioned above, on which aseismic slip has been reported or inferred, are located within the Lower Gutingkeng mudstone formation. These soft sediments seem to be rich in fluids, likely over-pressurized, and could explain the existence of active mud volcanoes along active faults in southwestern Taiwan (Yuan et al. 1987; Sun et al. 2010; Huang et al. 2016a). In the Coastal Plain north of the Tainan anticline, seismic lines D1 and D5 suggest that Lower Gutingkeng formation behaves as a basal pure-shear layer (Marc et al. 2010; Fig. 7c). We interpret that the friction in this layer could be too low to accumulate much tectonic strain, so that faults located within this layer are able to slip interseismically and are easily triggered by other earthquakes.

5. CONCLUSIONS

In spite of evidence for tectonic activity at different depths, from the shallow upper crust down to 15 - 20 km depth where the Meinong earthquake nucleated, relatively straightforward relationships could be drawn between sharper gradients in coseismic surface displacement during the Meinong earthquake and shallow geological structures. This allowed us to determine qualitatively which structures were or may have been triggered in the earthquake. These structures are mainly the ramp beneath the Lungchuan ridge, the Lungchuan backthrust, and the Tainan detachment. The Tainan detachment may have slipped as far west as below the Tainan Tableland, triggering minor slip on the Pitou backthrust and the Houchiali fault. Testing these inferences by estimating triggered slip on such complex fault geometries, also accounting for the possible inelastic deformation in the Gutingkeng formation, challenges the ability of current numerical modeling techniques.

The structures triggered during the Meinong earthquake are structurally connected, thus faults activation may consist in simple slip partitioning from the ramp and detachment onto the backthrusts that root on the detachment. However, the structural connection and triggering mechanism between the shallow structures and the deep source remain to be explained. Retrieving that connection may rely on increased efforts towards seismic instrumentation in order to investigate micro-seismicity and improve the resolution of upper crustal structure imaging techniques.

Acknowledgements We are grateful to Ling-Ho Chung, Antoine Poujol, De-Cheng Yi for discussions and/or help during the field survey, and to Wen-Shan Chen, Hsin Tung, and Jonathan E. Wu for discussions during this work. This manuscript benefited from comments from two anonymous reviewers. We acknowledge the geodesy survey and processing teams supported by Central Geological Survey of Taiwan (MOEA) and the GPS laboratory at the Institute of Earth Sciences, Academia Sinica, Taiwan (continuous GPS time series downloaded from http://gps.earth.sinica.edu.tw). Most figures in this manuscript were designed using GMT software (Wessel and Smith 1991). Simple structural models were run using the FFF program of Rick Allmendinger. This research was mainly supported by the Taiwan Ministry of Science and Technology, grant number MOST104-2116-M-008-025-MY3 and appointment to M. Le Béon. Part of this research was supported by the NASA Earth Surface and Interior focus area and performed at the Jet Propulsion Laboratory, California Institute of Technology. M.-H. Huang is supported by an appointment to the NASA Postdoctoral Program at the Jet Propulsion Laboratory, administered by the Universities Space and Research Association through a contract with NASA. B. Fruneau and E. Pathier were supported by the French spatial agency CNES (TOSCA project Tersol Glob-Taiwan) and by the France-Taiwan Hubert-Curien Program Orchid.

REFERENCES

Allen, C. R., M. Wyss, J. N. Brune, A. Grantz, and R. E. Wallace, 1972: Displacements on the Imperial, Superstition Hills and San Andreas faults triggered by the

Borrego Mountain earthquake. U.S. Geological Survey Professional Paper, No. 787, 87-104, Washington, D.C.

Berberian, M., J. A. Jackson, E. Fielding, B. E. Parsons, K. Priestley, M. Qorashi, M. Talebian, R. Walker, T. J. Wright, and C. Baker, 2001: The 1998 March 14 Fandoqa earthquake (M_w6.6) in Kerman province, southeast Iran: re-rupture of the 1981 Sirch earthquake fault, triggering of slip on adjacent thrusts and the active tectonics of the Gowk fault zone. *Geophys. J. Int.*, **146**, 371-398, doi: 10.1046/j.1365-246x.2001.01459.x. [Link]

Bodin, P., R. Bilham, J. Behr, J. Gomberg, and K. W. Hudnut, 1994: Slip triggered on southern California faults by the 1992 Joshua Tree, Landers, and big bear earthquakes. *Bull. Seismol. Soc. Am.*, **84**, 806-816.

Bonilla, M. G., 1975: A review of recently active faults in Taiwan. U.S. Geological Survey Open-File Report, 75-41, 43 pp.

Camanni, G., J. Alvarez-Marron, D. Brown, C. Ayala, Y. M. Wu, and H. H. Hsieh, 2016: The deep structure of south-central Taiwan illuminated by seismic tomography and earthquake hypocenter data. *Tectonophysics*, **679**, 235-245, doi: 10.1016/j.tecto.2015.09.016. [Link]

Carena, S., J. Suppe, and H. Kao, 2002: Active detachment of Taiwan illuminated by small earthquakes and its control of first-order topography. *Geology*, **30**, 935-938, doi: 10.1130/0091-7613(2002)030<0935:ADOTIB>2.0.CO;2. [Link]

Central Geological Survey, 2010: Active fault map of Taiwan.

Central Geological Survey, 2014: Report on geodetic monitoring of active faults 2/4. Ministry of Economic Affairs, Taiwan, R.O.C. (in Chinese)

Central Geological Survey, 2016: Report on the 2016/02/06 Earthquake (in Chinese). Ministry of Economic Affairs, Taiwan, R.O.C.

Chinese Petroleum Corporation, 1989: Geological map of Tai-Nan, scale 1:100,000. Taiwan Petroleum Exploration Division, Chinese Petroleum Corporation, Taiwan, R.O.C.

Ching, K. E., R. J. Rau, K. M. Johnson, J. C. Lee, and J. C. Hu, 2011a: Present-day kinematics of active mountain building in Taiwan from GPS observations during 1995-2005. *J. Geophys. Res.*, **116**, B09405, doi: 10.1029/2010JB008058. [Link]

Ching, K. E., M. L. Hsieh, K. M. Johnson, K. H. Chen, R. J. Rau, and M. Yang, 2011b: Modern vertical deformation rates and mountain building in Taiwan from precise leveling and continuous GPS observations, 2000-2008. *J. Geophys. Res.*, **116**, B08406, doi: 10.1029/2011JB008242. [Link]

Ching, K. E., K. M. Johnson, R. J. Rau, R. Y. Chuang, L. C. Kuo, and P. L. Leu, 2011c: Inferred fault geometry and slip distribution of the 2010 Jiashian, Taiwan, earthquake is consistent with a thick-skinned deformation model. *Earth Planet. Sci. Lett.*, **301**, 78-86, doi: 10.1016/j.epsl.2010.10.021. [Link]

Chung, C. T., 1968: Regional stratigraphic and structural study of the Tainan foothills area, southern Taiwan. *Petrol. Geol. Taiwan*, **6**, 15-31.

Cruikshank, K. M., A. M. Johnson, R. W. Fleming, and R. Jones, 1996: Winnetka deformation zone: Surface expression of coactive slip on a blind fault during the Northridge earthquake sequence, California. U.S. Geological Survey Open-File Report, NO. 96-698, 70 pp.

Doin, M. P., C. Lasserre, G. Peltzer, O. Cavalié, and C. Doubre, 2009: Corrections of stratified tropospheric delays in SAR interferometry: Validation with global atmospheric models. *J. Appl. Geophys.*, **69**, 35-50, doi: 10.1016/j.jappgeo.2009.03.010. [Link]

Doin, M. P., F. Lodge, S. Guillaso, R. Jolivet, C. Lasserre, G. Ducret, R. Grandin, E. Pathier, and V. Pinel, 2011: Presentation of the small baseline NSBAS processing chain on a case example: the Etna deformation monitoring from 2003 to 2010 using ENVISAT data. Proc. Fringe symposium, Frascati, Italy, ESA SP-697.

Du, W. X., L. R. Sykes, B. E. Shaw, and C. H. Scholz, 2003: Triggered aseismic fault slip from nearby earthquakes, static or dynamic effect? *J. Geophys. Res.*, **108**, 2131, doi: 10.1029/2002JB002008. [Link]

Ducret, G., M. P. Doin, R. Grandin, C. Lasserre, and S. Guillaso, 2014: DEM Corrections before unwrapping in a small baseline strategy for InSAR time series analysis. *IEEE Geosci. Rem. Sens. Lett.*, **11**, 696-700, doi: 10.1109/LGRS.2013.2276040. [Link]

Epard, J. L. and R. H. Groshong, 1995: Kinematic model of detachment folding including limb rotation, fixed hinges and layer-parallel strain. *Tectonophysics*, **247**, 85-103, doi: 10.1016/0040-1951(94)00266-C. [Link]

Freed, A. M., 2005: Earthquake triggering by static, dynamic, and post-seismic stress transfer. *Annu. Rev. Earth Planet. Sci.*, **33**, 335-67, doi: 10.1146/annurev.earth.33.092203.122505. [Link]

Fruneau, B., E. Pathier, D. Raymond, B. Deffontaines, C. T. Lee, H. T. Wang, J. Angelier, J. P. Rudant, and C. P. Chang, 2001: Uplift of Tainan Tableland (SW Taiwan) revealed by SAR interferometry. *Geophys. Res. Lett.*, **28**, 3071-3074, doi: 10.1029/2000GL012437. [Link]

Geotechnical Extreme Event Reconnaissance (GEER) Association, 2014: Geotechnical engineering reconnaissance of the August 24, 2014 M6 South Napa Earthquake. Report of the NSF Sponsored GEER Association Team, California Geological Survey, Pacific Earthquake Engineering Research Center and U.S. Geological Survey, GEER-037.

Goto, H, H. Tsutsumi, S. Toda, and Y. Kumahara, 2017: Geomorphic features of surface ruptures associated

with the 2016 Kumamoto earthquake in and around the downtown of Kumamoto City, and implications on triggered slip along active faults. *Earth Planets Space*, **69**, 1-12, doi: 10.1186/s40623-017-0603-9. [Link]

Grandin, R., M. P. Doin, L. Bollinger, B. Pinel-Puysségur, G. Ducret, R. Jolivet, and S. N. Sapkota, 2012: Long-term growth of the Himalaya inferred from interseismic InSAR measurement. *Geology*, **40**, 1059-1062, doi: 10.1130/G33154.1. [Link]

Hardy, S. and R. W. Allmendinger, 2009: Trishear: A review of kinematics, mechanics, and applications. In: McClay, K., J. Shaw, and J. Suppe (Eds.), Thrust Faukt-Related Folding, AAPG, Tulsa, Okla, 95-119, doi: 10.1306/13251334M943429. [Link]

Hearn, E. H. and R. Bürgmann, 2005: The effect of elastic layering on inversions of GPS data for earthquake slip and stress changes: Strike-Slip Earthquakes. *Bull. Seism. Soc. Am.*, **95**, 1637-1653, doi: 10.1785/0120040158. [Link]

Hsu, Y. J., S. B. Yu, M. Simons, L. C. Kuo, and H. Y. Chen, 2009: Interseismic crustal deformation in the Taiwan plate boundary zone revealed by GPS observations, seismicity, and earthquake focal mechanisms. *Tectonophysics*, **479**, 4-18, doi: 10.1016/j.tecto.2008.11.016. [Link]

Hsu, Y. J., S. B. Yu, L. C. Kuo, Y. C. Tsai, and H. Y. Chen, 2011: Coseismic deformation of the 2010 Jiashian, Taiwan earthquake and implications for fault activities in southwestern Taiwan. *Tectonophysics*, **502**, 328-335, doi: 10.1016/j.tecto.2011.02.005. [Link]

Huang, I. J., 2013: Study of the relationship between surface rupture and faulting in relation to Jiashian earthquake. Master Thesis, National Central University, Taoyuan City, Taiwan, 315 pp. (in Chinese)

Huang, M. H., J. C. Hu, C. S. Hsieh, K. E. Ching, R. J. Rau, E. Pathier, B. Fruneau, and B. Deffontaines, 2006: A growing structure near the deformation front in SW Taiwan as deduced from SAR interferometry and geodetic observation. *Geophys. Res. Lett.*, **33**, L12305, doi: 10.1029/2005GL025613. [Link]

Huang, M. H., J. C. Hu, C. S. Hsieh, K. E. Ching, R. J. Rau, E. Pathier, B. Fruneau, and B. Deffontaines, 2009: Active deformation of Tainan Tableland of southwestern Taiwan based on geodetic measurements and SAR interferometry. *Tectonophysics*, **466**, 322-334, doi: 10.1016/j.tecto.2007.11.020. [Link]

Huang, M. H., D. Dreger, R. Bürgmann, S. H. Yoo, and M. Hashimoto, 2013: Joint inversion of seismic and geodetic data for the source of the 2010 March 4, Mw 6.3 Jia-Shian, SW Taiwan, earthquake. *Geophys. J. Int.*, **193**, 1608-1626, doi: 10.1093/gji/ggt058. [Link]

Huang, M. H., H. Tung, E. J. Fielding, H. H. Huang, C. Liang, C. Huang, and J. C. Hu, 2016a: Multiple fault slip triggered above the 2016 Mw 6.4 MeiNong earthquake in Taiwan. *Geophys. Res. Lett.*, **43**, 7459-7467, doi: 10.1002/2016GL069351. [Link]

Huang, M. H., R. Bürgmann, and J. C. Hu, 2016b: Fifteen years of surface deformation in Western Taiwan: Insight from SAR interferometry. *Tectonophysics*, **692**, 252-264, doi: 10.1016/j.tecto.2016.02.021. [Link]

Huang, S. T., K. M. Yang, J. H. Hung, J. C. Wu, H. H. Ting, W. W. Mei, S. H. Hsu, and M. Lee, 2004: Deformation front development at the northeast margin of the Tainan basin, Tainan-Kaohsiung area, Taiwan. *Mar. Geophys. Res.*, **25**, 139-156, doi: 10.1007/s11001-005-0739-z. [Link]

Huang, W. J. and A. M. Johnson, 2010: Quantitative description and analysis of earthquake-induced deformation zones along strike-slip and dip-slip faults. *J. Geophys. Res.*, **115**, B03408, doi: 10.1029/2009JB006361. [Link]

Johnson, A. M., R. W. Fleming, K. M. Cruikshank, and R. F. Packard, 1996: Coactive fault of the Northridge earthquake-Granada Hills area. U.S. Geological Survey Open File Report, No. 96-523, 66 pp, California.

Jolivet, R., R. Grandin, C. Lasserre, M. P. Doin, and G. Peltzer, 2011: Systematic InSAR tropospheric phase delay corrections from global meteorological reanalysis data. *Geophys. Res. Lett.*, **38**, L17311, doi: 10.1029/2011GL048757. [Link]

Kanamori, H., L. Ye, B.-S. Huang, H.-H. Huang, S.-J. Lee, W.-T. Liang, Y.-Y. Lin, K.-F. Ma, Y.-M. Wu, and T.-Y. Yeh, 2017: A strong-motion hot spot of the 2016 Meinong, Taiwan, earthquake (M_w = 6.4). *Terr. Atmos. Ocean. Sci.*, **28**, 637-650, doi: 10.3319/TAO.2016.10.07.01. [Link]

Kao, H. and W. P. Chen, 2000: The Chi-Chi earthquake sequence: Active, out-of-sequence thrust faulting in Taiwan. *Science*, **288**, 2346-2349, doi: 10.1126/science.288.5475.2346. [Link]

Le Béon, M., O. Marc, M. H. Huang, S. T. Huang, J. Suppe, and R. F. Chen, 2014: Deep structure and deformation history of the rapidly growing Tainan anticline, southwestern Taiwan. Geodynamics and Environment in East Asia International Conference, 7th Taiwan-France Earth Science Symposium, Hualien, Taiwan. (in Chinese)

Lee, S. J., T. Y. Yeh, and Y. Y. Lin, 2016: Anomalously Large Ground Motion in the 2016 M_L 6.6 Meinong, Taiwan, Earthquake: A Synergy Effect of Source Rupture and Site Amplification. *Seismol. Res. Lett.*, **87**, 1319-1326, doi: 10.1785/0220160082. [Link]

Lin, K. C., J. C. Hu, K. E. Ching, J. Angelier, R. J. Rau, S. B. Yu, C. H. Tsai, T. C. Shin, and M. H. Huang, 2010: GPS crustal deformation, strain rate, and seismic activity after the 1999 Chi-Chi earthquake in Taiwan. *J. Geophys. Res.*, **115**, B07404, doi: 10.1029/2009JB006417. [Link]

Lin, K. C., B. Delouis, J. C. Hu, L. M. Nocquet, and L. Mozziconacci, 2015: Reassessing the complexity of the rupture of the 2010 Jia-Shian Earthquake (Mw 6.2) in Southwestern Taiwan by inverting jointly teleseismic, strong-motion and CGPS data. *Tectonophysics*, **692**, 278-294, doi: 10.1016/j.tecto.2015.09.015. [Link]

Marc, O., J. Suppe, S. Huang, M. Le Béon, M. H. Huang, and J. C. Hu, 2010: Deep structure and deformation history of the rapidly growing Tainan anticline, southwestern Taiwan. AGU Fall Meeting, San Francisco, USA.

Mouthereau, F. and O. Lacombe, 2006: Inversion of the Paleogene Chinese continental margin and thick-skinned deformation in the Western Foreland of Taiwan. *J. Struct. Geol.*, **28**, 1977-1993, doi: 10.1016/j.jsg.2006.08.007. [Link]

Mouthereau, F., O. Lacombe, B. Deffontaines, J. Angelier, and S. Brusset, 2001: Deformation history of the southwestern Taiwan foreland thrust belt: insights from tectono-sedimentary analyses and balanced cross-sections. *Tectonophysics*, **333**, 293-318, doi: 10.1016/S0040-1951(00)00280-8. [Link]

National Earthquake Information Center, 2016: M6.4-Taiwan, United States Geological Survey, 2016. Available at http://earthquake.usgs.gov/earthquakes/eventpage/us20004y6h#scientific.

Pan, Y. S., 1968: Interpretation and seismic coordination of the Bouguer gravity anomalies obtained in southwestern Taiwan. *Petrol. Geol. Taiwan*, **6**, 197-208.

Pathier, E., B. Fruneau, B. Deffontaines, J. Angelier, C. P. Chang, S. B. Yu, and C. T. Lee, 2003: Coseismic displacements of the footwall of the Chelungpu fault caused by the 1999, Taiwan, Chi-Chi earthquake from InSAR and GPS data. *Earth Planet. Sci. Lett.*, **212**, 73-88, doi: 10.1016/S0012-821X(03)00244-9. [Link]

Pathier, E., B. Fruneau, M. P. Doin, Y. T. Liao, J. C. Hu, and J. Champenois, 2014: What are the tectonic structures accommodating the present-day tectonic deformation in South-Western Taiwan? A new interpretation from ALOS-1 InSAR and GPS interseismic measurements. Geodynamics and Environment in East-Asia. 7th France-Taiwan Earth Sciences Symposium, Hualien, Taiwan.

Price, E. J. and D. T. Sandwell, 1998: Small-scale deformations associated with the 1992 Landers, California, earthquake mapped by synthetic aperture radar interferometry phase gradients. *J. Geophys. Res.*, **103**, 27001-27016, doi: 10.1029/98JB01821. [Link]

Rodriguez-Roa, F. A. and D. V. Wiltschko, 2010: Thrust belt architecture of the central and southern Western Foothills of Taiwan. *Geol. Soc. Lond. Spec. Publ.*, **348**, 137-168, doi: 10.1144/SP348.8. [Link]

Rymer, M. J., J. A. Treiman, K. J. Kendrick, J. J. Lienkaemper, R. J. Weldon, R. Bilham, M. Wei, E. J. Fielding, J. L. Hernandez, B. P. E. Olson, P. J. Irvine, N. Knepprath, R. R. Sickler, X. Tong, and M. E. Siem, 2010: Triggered surface slips in southern California associated with the 2010 El Mayor-Cucapah, Baja California, Mexico, earthquake. U.S. Geological Survey Open-File Report, No. 2010-1333, Reston, V. A., 72 pp.

Shaw, J. H., C. Connors, and J. Suppe, 2005: Seismic Interpretation of Contractional Fault-Related Folds, AAPG Seismic Atlas: AAPG Studies in Geology, Vol. 53, Tulsa, Oklahoma, U.S.A., 156 pp.

Shyu, J. B. H., Y. R. Chuang, Y. L. Chen, Y. R. Lee, and C. T. Cheng, 2016: A new on-land seismogenic structure source database from the Taiwan Earthquake Model (TEM) project for seismic hazard analysis of Taiwan. *Terr. Atmos. Ocean. Sci.*, **27**, 311-323, doi: 10.3319/TAO.2015.11.27.02(TEM). [Link]

Sun, C. H, S. C. Chang, C. L. Kuo, J. C. Wu, P. H. Shao, and J. N. Oung, 2010: Origins of Taiwan's mud volcanoes: Evidence from geochemistry. *J. Asian Earth Sci.*, **37**, 105-116, doi: 10.1016/j.jseaes.2009.02.007. [Link]

Suppe, J., 1980: Imbricated Structure of Western Foothills Belt, Southcentral Taiwan. *Petrol. Geol. Taiwan*, **17**, 1-16

Suppe, J., 1984: Kinematics of arc-continent collision, flipping of subduction, and back-arc spreading near Taiwan. *Mem. Geol. Soc. China*, **6**, 21-33.

Suppe, J. and D. A. Medwedeff, 1990: Geometry and kinematics of fault-propagation folding. *Eclogae Geol. Helv.*, **83**, 409-454.

Suppe, J., C. D. Connors, and Y. Zhang, 2004: Shear fault-bend folding. In: McClay, K. R. (Ed.), Thrust Tectonics and Hydrocarbon Systems, AAPG Memoir 82, 303-323.

Tsai, M. C., S. B. Yu, T. C. Shin, K. W. Kuo, P. L. Leu, C. H. Chang, and M. Y. Ho, 2015: Velocity field derived from Taiwan Continuous GPS Array (2007 - 2013). *Terr. Atmos. Ocean. Sci.*, **26**, 527-556, doi: 10.3319/TAO.2015.05.21.01(T). [Link]

Tung, H., Y.-S. Li, H.-Y. Chen, Y.-J. Hsu, and J.-C. Hu, 2016: Coseismic deformation of the 2016 Meinong earthquake revealed from GNSS and InSAR data. Taiwan Geosciences Assembly, Taipei, Taiwan, 16-20 May 2016, abstract.

Wei, M., D. Sandwell, Y. Fialko, and R. Bilham, 2011: Slip on faults in the Imperial Valley triggered by the 4 April 2010 Mw 7.2 El Mayor-Cucapah earthquake revealed by InSAR. *Geophys. Res. Lett.*, **38**, L01308, doi: 10.1029/2010GL045235. [Link]

Wen, S., Y.-L. Yeh, Y.-Z. Chang, and C.-H. Chen, 2017: The seismogenic process of the 2016 Meinong earthquake, southwest Taiwan. *Terr. Atmos. Ocean. Sci.*, **28**, 651-662, doi: 10.3319/TAO.2017.02.17.01. [Link]

Wessel, P. and W. Smith, 1991: Free software helps map and display data. *Eos Trans. AGU*, **72**, 445-446, doi: 10.1029/90EO00319. [Link]

Wright, T., E. Fielding, and B. Parsons, 2001: Triggered slip: Observations of the 17 August 1999 Izmit (Turkey) Earthquake using radar interferometry. *Geophys. Res. Lett.*, **28**, 1079-1082, doi: 10.1029/2000GL011776. [Link]

Yu, H. L., H. H. Shih, C. S. Huang, C. G. Ho, and B. S. Tseng, 1990: Geological review of the Lungchuan structure, Tainan and Kengnei, Shiaokunshui structure, Kaohsiung. Chinese Petroleum Corporation, R.O.C. (in Chinese)

Yuan, J., S. T. Huang, T. F. Chou, J. C. Wu, and D. L. Lu, 1987: The origin of the abnormal pressure zones in Southwestern Taiwan. *Ann. Explor. Prod.*, **10**, 1-27. (in Chinese)